Research Article

$SnO_x/Ag/SnO_x$ heat-reflector coatings prepared by DC sputtering

C. Guillén[1] · J. Herrero[1]

Received: 22 April 2020 / Accepted: 14 September 2020 / Published online: 23 September 2020

Abstract
Transparent heat reflectors have been prepared by DC sputtering of pure metal targets on glass substrates at room temperature. These are three-layer coatings based on a high reflective silver film surrounded by transparent tin oxide layers, which reduce greatly the silver reflection in the visible range, but not in the infrared region. In fact, such infrared reflectance has been controlled by the Ag interlayer thickness. Besides, during the tin oxide growth by reactive deposition, both the oxygen partial pressure and the sputtering time have been tuned to maximize the visible transmission while avoiding the possible Ag oxidation. In this way, optimized $SnO_x/Ag/SnO_x$ coatings have been achieved with high luminous transmittance ($\tau_L = 81\%$ including the glass substrate) and low solar heat gain ($g = 0.55$), as required for energy-efficient glazing applications.

Keywords Silver · Tin oxide · Thin films · Transparent heat reflectors · Solar control

1 Introduction

Nowadays, several glazing technologies are being developed to improve the energy performance of buildings. In particular, researches in thin-film coatings are focused on spectrally selective glazing systems [1, 2]. Conventional glass windows (without any coating) allow crossing visible transmittance, as well as solar heat that increases the temperature inside the building. However, a functional coating on the glass can eliminate solar heat and reduce the cooling energy consumption. For this purpose, heat regulating materials should be transparent in the visible region and highly reflective in the infrared spectrum [1]. Moreover, a high infrared reflectance is related to a low radiative heat transfer (low-emittance) that is beneficial not only to reduce cooling needs in the summer, but also to decrease heating costs in the winter by minimizing the heat radiation to the outside [3]. In general, low-emittance coatings have a high reflectance in the far infrared (at wavelengths above 15 µm) and they include a subcategory according to their reflectance values in the near infrared. The so-called solar control coatings have also a high reflectance in the near infrared range of the solar spectrum (at 0.7–2.5 µm wavelengths) [4]. This is particularly beneficial in hot climates, but some transmission of the infrared solar radiation can be preferred for buildings located in cold regions [5].

Solar control coatings (or transparent heat reflectors) are typically constituted by thin layers of metals or metal oxides with a high free-carrier density [4]. For such conductive metal oxides, the thermal absorption is located in the near infrared region, which reduces their maximum infrared reflectance [6]. For metals, the thermal absorption is usually placed in the near ultraviolet, although they have higher extinction coefficients than metal oxides. Besides, for very thin metal thicknesses (below the percolation threshold) the formation of an island structure produces plasmonic absorption in the visible region [7]. The minimal thickness to achieve a continuous metal film with low visible absorption is highly dependent on the substrate characteristics and other deposition parameters [8, 9]. Among metals, Ag is preferred because it has the lowest visible absorption, whereas

✉ C. Guillén, c.guillen@ciemat.es | [1]Departamento de Energía (CIEMAT), Avda. Complutense 40, 28040 Madrid, Spain.

others like Au or Cu show some coloration that is undesired for many architectural applications [4]. In order to suppress its visible reflectance, the metal layer (M) is combined with dielectric films (D), serving essentially for antireflection purposes. Several bilayer configurations (D/M or M/D) are proven effective in enhancing the overall visible transmittance [10] and also the infrared reflectance by smoothing the metal surface [11]. Nevertheless, only the three-layer system D/M/D allows achieving maximum transmittance above 80% at wavelengths near $\lambda = 0.55$ µm (which corresponds to the human eye peak sensitivity) by a fine adjustment of the thickness for each layer [12, 13].

The challenges to improve D/M/D coatings are a design of the multilayer and growth of high-quality metal thin film. A symmetrical design, with undercoat and overcoat dielectric layers of identical thickness, is found optimal [12, 13]. In the visible range, the refractive index (n) of the dielectric layers should match the extinction coefficient (k) of the metallic reflector [14]. Silver films have $k \sim 3.5$ at $\lambda = 0.55$ µm [15, 16] and combine well with TiO_2 ($n \sim 2.2$) [16], SnO_2 ($n \sim 2.0$) and ZnO ($n \sim 1.9$) [17]. It is known that smaller refractive indices allow wider transmission regions at the cost of a more gradual transition and smaller infrared reflectivity [18]. Besides, it should be noted that for a same material the refractive index value changes with the film thickness and other deposition conditions [1, 17]. D/M/D multilayers for architectonical applications are generally prepared on glass substrates by magnetron sputtering [2, 5], owing to its capability for the large-scale processing [19]. The ion bombardment effects associated with this technique contribute to smooth the surface of the first dielectric film and hence to improve the quality of the metal overlayer. However, an additional barrier film is necessary to protect the metal-reflector from oxidation during the deposition of the second dielectric layer, in particular when it is performed by reactive DC sputtering from metallic targets [17, 20]. This sputtering mode has economic advantages due to simple equipment, but it requires a fine control of the reactive parameters, mainly the power density and the oxygen to argon partial pressures ratio.

In the present work, D/M/D multilayers based on silver and tin oxide thin films have been developed by DC sputtering from pure metal targets. Especially during the last tin oxide growth, the oxygen partial pressure has been tuned to maximize the dielectric film transmission while avoiding Ag underlayer oxidation. In this way, a good performance is achieved without any additional barrier layer. For both silver and tin oxide single-films, the optical properties have been analyzed as a function of the thickness and other deposition conditions. In the three-layer system, the thickness of the films has been changed to give high infrared reflection and low visual loss, as required for energy-efficient glazing applications.

2 Methods

Thin films of silver and tin oxide were prepared onto borosilicate glass substrates by means of an in-line sputtering system operating at room temperature. The system has two connected chambers, one with a Sn target (99.99% purity) and the other with an Ag target (99.99% purity), attached to respective DC power sources, and a carrier for the substrates that can be moved in vacuum between chambers. The silver sputtering process was performed in pure argon atmosphere, at a constant deposition rate of 6 nm/min. For the tin oxide growth, oxygen was introduced as a reactive gas during sputtering of the Sn target, varying the oxygen to argon partial pressure ratio (O_{pp}) in the 14–20% range. This changes the film stoichiometry from SnO to a mixture of SnO and SnO_2 when the oxygen proportion increases, but Sn and SnO coexist for $O_{pp} \leq 12\%$, as demonstrated in a previous work [21]. The power density was adjusted to give a deposition rate of 20 nm/min for the tin oxide layers, whereas the sputtering time was varied to obtain different thickness values for both silver and tin oxide films. Other experimental details are summarized in Table 1.

Optical measurements of the samples were done with unpolarized light at normal incidence in the wavelength range from 0.25 to 2.50 µm, with a double beam spectrophotometer Perkin–Elmer Lambda 9, taking the air as reference. The spectrophotometer is equipped with an integrating sphere that allows total reflectance (R) and transmittance (T) measurements [22]. These data have been used to assess the influence of deposition parameters in order to achieve the desired optical properties (maximum visible transmittance, maximum infrared reflectance) for single-layer and multi-layer coatings.

In order to determine the optical constants of the isolated films, the measured transmittance is corrected by discounting the substrate contribution: $T_c(\%) = 100\ T(\%)/T_{glass}(\%)$. Then, the extinction coefficient

Table 1 Experimental conditions of sputtering deposition

Target	Base pressure	O_2 pressure	Working pressure (O_2+Ar)	Power density
Sn disk (Ø 15 cm)	$4*10^{-4}$ Pa	$(6–9)*10^{-2}$ Pa	0.45 Pa	0.6 W/cm^2
Ag disk (Ø 15 cm)	$4*10^{-4}$ Pa	–	0.45 Pa	0.2 W/cm^2

(k) and the refractive index (n) are calculated for the layers with different thickness (t) using the equations [23]:

$$k = -\frac{\lambda}{4\pi t} \ln\left\{0.01T_c(\%)\right\} \quad (1)$$

$$n = \left(\frac{1 + 0.01R(\%)}{1 - 0.01R(\%)}\right) + \left[\frac{0.04R(\%)}{(1 - 0.01R(\%))^2} - k^2\right]^{1/2} \quad (2)$$

Structures and thicknesses of the multilayer designs were analyzed by atomic force microscopy (AFM) with a Park XE-100 system, which has a separate sample stage for the X–Y scanning from the Z-scanner for height measurements. The lens for a CCD camera can be moved together with the Z-scanner in the vertical direction, so that the sample surface is focused before the cantilever is set to engage to the working distance. This allows for cross-section imaging with a spatial resolution in the nanometer range [24].

Besides, the solar glazing factors (luminous transmittance, emissivity, solar heat gain) have been calculated according to the European normative about glass in buildings [25]. Finally, a figure of merit (selectivity index) has been applied to compare the obtained coatings as energy-efficient windows.

3 Results and discussion

3.1 Influence of coating deposition parameters

In the first approximation, several D/Ag/D coatings were prepared by fixing the thickness of the layers within the range recommended from numerical simulations [12], specifically at 12 nm for Ag and 30 nm for each dielectric, but changing the oxygen partial pressure used for the dielectric tin oxide growth. The effect of this deposition parameter on the transmittance and reflectance spectra is illustrated in Fig. 1, for single dielectric films prepared at 18% O_{pp} (D1) or 14% O_{pp} (D2) as well as for the respective multilayers D1/Ag/D1 and D2/Ag/D2. These tin oxide layers should be considered as SnO_x, that is a mixture of SnO and SnO_2, with the x value increasing in the 1.0–1.4 interval when the oxygen partial pressure increases in the 14–18% range [21]. Due to the band gap energy is higher for SnO_2 ($E_g \sim 3.5$ eV) than for SnO ($E_g \sim 2.8$ eV) [21], the increment in the oxygen content makes to increase the optical transmittance at low wavelengths ($\lambda < 0.50$ µm). This fact is clearly seen in Fig. 1, which shows an improvement in visible transmittance that is higher for the single D1 film than for the respective D1/Ag/D1 coating. In the infrared region, identical behavior is observed for the D1 and D2 samples, but it changes

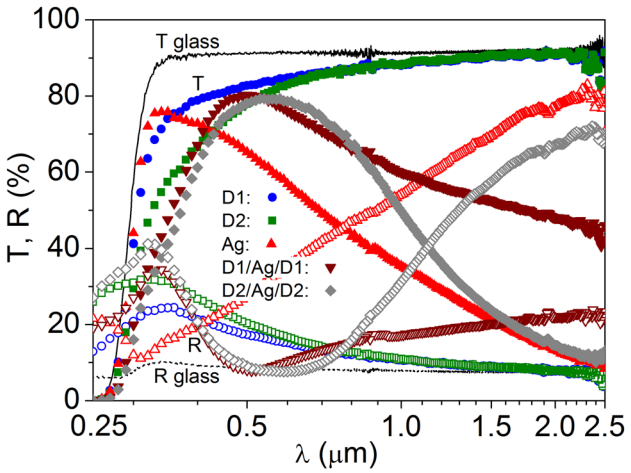

Fig. 1 Transmittance and reflectance spectra for different coatings grown on glass substrates: 30 nm-thick SnO_x films prepared at 18% O_{pp} (D1) or 14% O_{pp} (D2), 12 nm-thick Ag film and the respective multilayers D1/Ag/D1 and D2/Ag/D2. Spectra corresponding to the bare glass substrate are also included

for the three-layer systems. A high infrared reflectance is only attained for the D2/Ag/D2 coating, with D2 prepared at 14% O_{pp}, because an increment in the oxygen partial pressure produces a significant silver oxidation that reduces the reflectivity. This glass/D2/Ag/D2 configuration achieves a maximum transmittance $T_{max} = 80\%$ at $\lambda = 0.55$ µm, with a maximum reflectance $R_{max} = 72\%$ at $\lambda \sim 2.50$ µm close to that obtained for the single Ag film. The same infrared reflectance was attained by a glass/D1/Ag/D2 configuration, but with the maximum transmittance displaced to a lower wavelength ($T_{max} = 80\%$ at $\lambda = 0.50$ µm). Analogous displacement was also obtained with symmetric D2/Ag/D2 samples by decreasing the thickness of each D2 layer from 30 to 20 nm. In the following ones, all the SnO_x films were deposited at 14% O_{pp}.

The influence of the thickness on the transmittance and reflectance spectra of single SnO_x and Ag layers is represented in Fig. 2. Owing to the optical measurements were performed by taking the air as reference, the characteristics of the bare glass substrate are also included. The glass absorbs the harmful ultraviolet radiation and shows a flat transmittance of 91% and flat reflectance of 8% over the visible and infrared solar spectrum. For SnO_x films with a thickness increasing from 20 to 50 nm, the optical transmittance at $\lambda = 0.55$ µm decreases from 85 to 75%, while the corresponding reflectance increases from 14 to 23%. For analogous Ag layers with thickness increasing from 15 to 24 nm, a faster change is observed in the visible transmittance (from 56 to 12% at $\lambda = 0.55$ µm) and reflectance (from 40 to 86% at the same wavelength). These abrupt variations in transmittance and reflectance indicate a

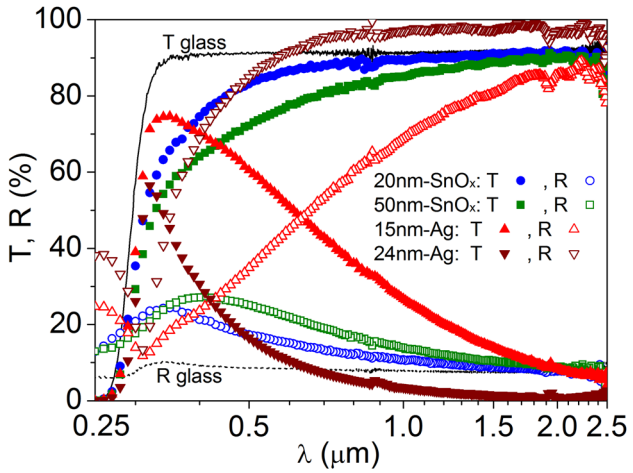

Fig. 2 Transmittance and reflectance spectra for various single-layer coatings on glass substrates: SnO_x films grown at 14%O_{pp} with 20 nm or 50 nm thickness, and Ag films with 15 nm or 24 nm thickness. Spectra for the bare glass substrate are included for comparison

significant dependence of the optical constants of the silver thin films on their thickness.

Figure 3 shows the evolution of k and n values as a function of the wavelength for the SnO_x and Ag samples represented in Fig. 2. At $\lambda = 0.55$ μm, the SnO_x films exhibit optical constants increasing from $n = 2.3$ and $k = 0.1$ for 20 nm thickness to $n = 2.9$ and $k = 0.2$ for the 50 nm thick film. These refractive index values are close to those reported for pure SnO layers [26], whereas SnO_2 has a smaller refractive index (below 2.0 at $\lambda = 0.55$ μm) [27]. For the present SnO_x samples, the decrease in refractive index can be related to a higher proportion of SnO_2 in thinner coatings, but also to a decrease in film density or the presence of some voids (being the air value $n_{air} = 1$ lower than n_{SnOx}). According to the Bruggeman effective-medium model [28], the fraction of voids for the thinnest SnO_x layer (in comparison with the thickest one) would be of 30%. A similar change of the layer density with the thickness is observed in other metal oxide thin films [17]. For the Ag samples an opposite variation is observed, with n decreasing from 0.8 to 0.4 and k increasing from 1.4 to 3.6 (at $\lambda = 0.55$ μm) when the thickness increases from 15 to 24 nm. The optical constants obtained for the thickest Ag film are near to those expected for bulk silver [15]. The increase in refractive index as the silver thickness decreases is also related to the presence of voids (with $n_{air} = 1$ higher than n_{Ag}). The fraction of voids estimated for the thinnest Ag layer (compared to the thickest film) is of 68%, which explains the decrease in the extinction coefficient as well. This allows maximizing the transmission of visible light by minimizing the extinction coefficient, but the Ag film must be thick enough to give a high infrared reflectance for heat reflecting applications.

For the three-layer coatings, the infrared reflectance is given by the Ag interlayer, while the visible transmittance depends on the thickness selected for the SnO_x films on both sides. The optical behavior is illustrated in Fig. 4 for several coatings with a fixed Ag interlayer thickness of 15 nm and different thicknesses for the SnO_x films. The highest transmittance values ($T_{max} = 85 \pm 1\%$ including the glass substrate) have been achieved with symmetrical configurations, that is with identical thickness for the lower and upper SnO_x films. Besides, the T_{max} position shifted to higher wavelengths when the SnO_x thickness increases. In

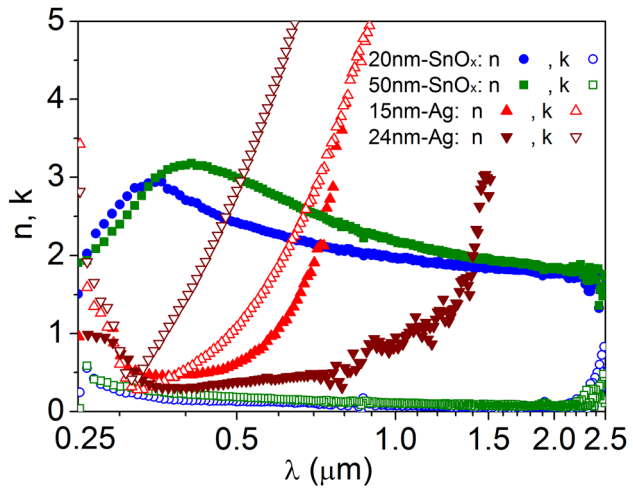

Fig. 3 Refractive index and extinction coefficients calculated from the optical data depicted in Fig. 2 for various single-layer coatings: SnO_x films grown at 14% O_{pp} with 20 nm or 50 nm thickness, and Ag films with 15 nm or 24 nm thickness

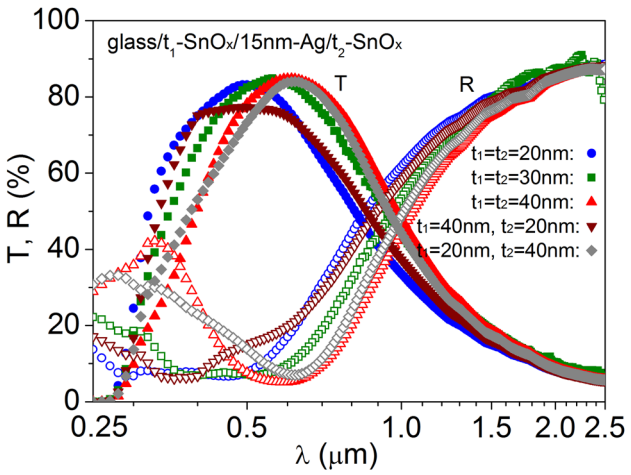

Fig. 4 Transmittance and reflectance spectra for three-layer coatings on glass substrates, with a same 15 nm-thick Ag interlayer and changing the thickness of SnO_x films in different ways

order to place the maximum transmittance at $\lambda = 0.55$ µm, the optimum dielectric thickness is set at 30 nm, lower than reported for analogous three-layer systems [16, 19, 29] taken into account that higher thickness values are required for dielectrics with lower refractive indexes [12]. For materials with similar extinction coefficients but different refractive indexes, the use of a minimum thickness allows a superior overall transmittance [12]. The high refractive index of the present SnO_x films, in comparison with pure SnO_2, ZnO or TiO_2 [16, 17], makes possible to achieve a high visible transmittance (85%) with a reduced dielectric thickness (30 nm of SnO_x). In other works, optimal D/Ag/D designs give $T_{max} \leq 80\%$ with symmetrical configurations using 46 nm thick TiO_2 layers [12, 14], 40 nm thick ZnO films [17] or 38 nm thick SnO_2 coatings [20].

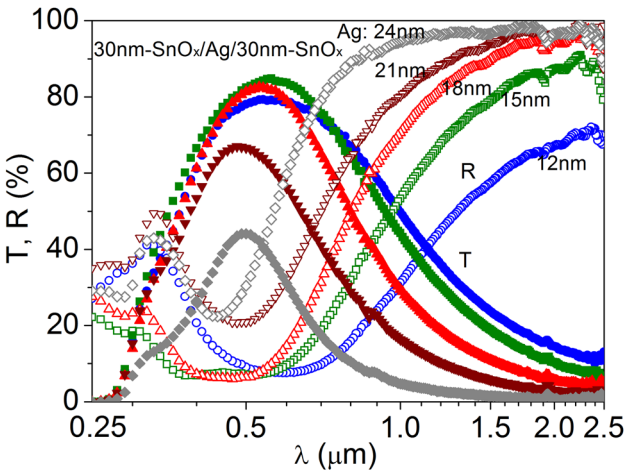

Fig. 5 Transmittance and reflectance spectra for three-layer coatings on glass substrates, with 30 nm-thick SnO_x films in symmetrical configuration and changing the thickness of the intermediate Ag layer

After setting the thickness of the internal and external SnO_x films at 30 nm, the evolution of the three-layer properties was analyzed as a function of the intermediate Ag film. Figure 5 shows that coatings with very thin Ag layers ($t_{Ag} < 15$ nm) do not exhibit the required heat reflectance. The infrared reflectance increases as the silver thickness increases, but a high visible transmittance (above 80% at 0.55 µm wavelength) is only maintained for $t_{Ag} < 21$ nm. For thicker silver films, both the bandwidth and the intensity of the visible transmittance decrease quickly as the minimum reflectance wavelength moves towards lower values when the Ag layer thickness rises. The same behavior has been observed for analogous D/Ag/D coatings with $t_{Ag} \geq 24$ nm and different dielectric materials [16, 30]. Here, the change is detected at lower t_{Ag} values, more according to the simulations [12]. This indicates that stable and sharp interfaces have been achieved, taking into account that the effective silver thickness could be reduced by diffusion and/or oxidation processes during the successive layers deposition [30]. Figure 6 shows AFM images comparing three-layer stacks with different Ag interlayer thicknesses. Besides, the optical spectral data, $T(\lambda)$ and $R(\lambda)$, depicted in Fig. 5 have been used in the following section to assess the suitability of the three-layer coatings for efficient glazing applications.

3.2 Evaluation of solar glazing factors

Incident solar radiation on the earth surface is illustrated in Fig. 7 for the reference spectrum AM1.5, which has 53% of the total irradiance in the visible region (from 0.38 µm to 0.78 µm), 4% in ultraviolet light (below 0.38 µm) and 43% in the infrared range (above 0.78 µm). For fenestration products, luminous transmittance and colorimetric calculations are based on the standard illuminant D65, which represents the typical spectral distribution of daylight at

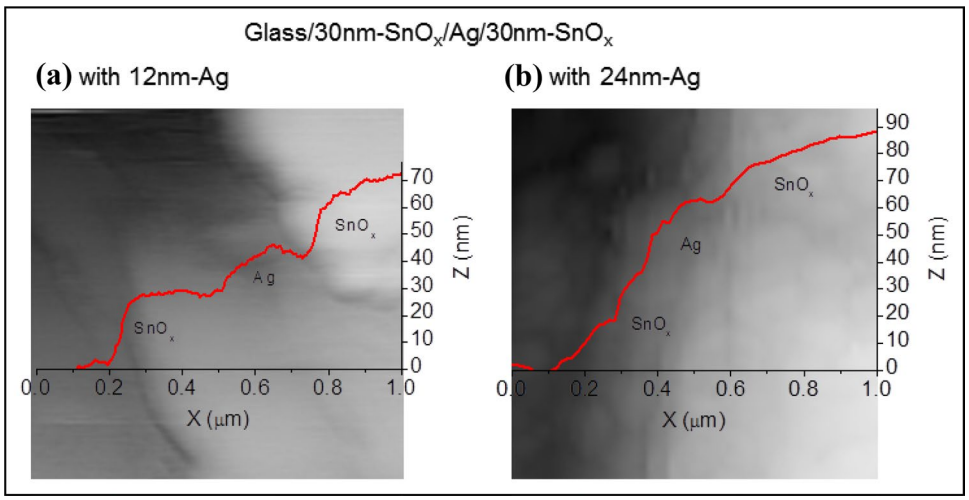

Fig. 6 Representative profiles for three-layer coatings with different Ag interlayer thicknesses, obtained from AFM images on 1 µm × 1 µm areas (X–Y scan)

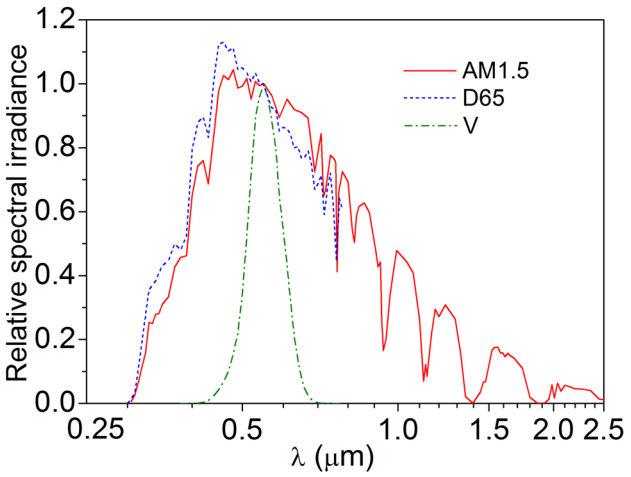

Fig. 7 Relative spectral distributions for the solar spectrum AM1.5 and the illuminant D65. These spectra are normalized to their value at 0.55 μm, which is the peak of the standard photopic vision V

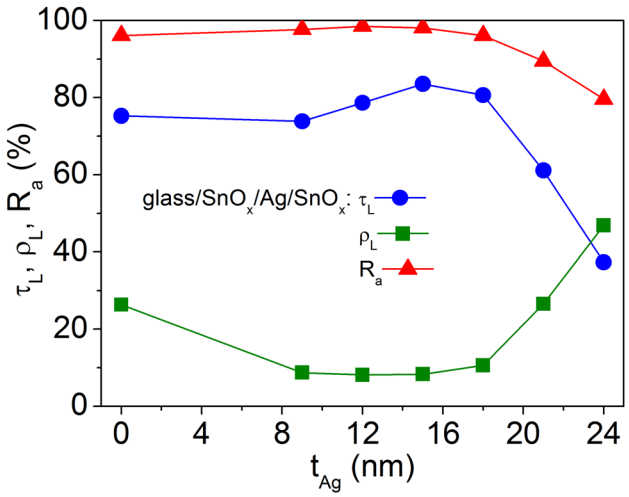

Fig. 8 Luminous transmittance, luminous reflectance and color rendering index calculated for three-layer coatings on glass substrates, with 30 nm-thick SnO_x films on both sides and different thickness for the Ag interlayer

a color temperature of 6500 K, related to clear conditions around noon at average latitudes in Europe [31]. A luminous efficiency function, the standard photopic vision $V(\lambda)$, is also used to describe the spectral sensitivity of the human eye, centered at $\lambda = 0.55$ μm as shown in Fig. 7. Thus, the luminous transmittance and reflectance (τ_L, ρ_L) denote the fraction of the incident light coming from the D65 illuminant that is transmitted or reflected by the glazing and is viewed by a standard photopic observer [25]:

$$\tau_L = \frac{\sum_{\lambda=0.38\mu m}^{0.78\mu m} T(\lambda) D_{65}(\lambda) V(\lambda) \Delta\lambda}{\sum_{\lambda=0.38\mu m}^{0.78\mu m} D_{65}(\lambda) V(\lambda) \Delta\lambda} \quad (3)$$

$$\rho_L = \frac{\sum_{\lambda=0.38\mu m}^{0.78\mu m} R(\lambda) D_{65}(\lambda) V(\lambda) \Delta\lambda}{\sum_{\lambda=0.38\mu m}^{0.78\mu m} D_{65}(\lambda) V(\lambda) \Delta\lambda} \quad (4)$$

Besides, the color rendering index (R_a) is used to quantify the ability of transmitted daylight through the glazing ($T(\lambda)$*D65) to portray a variety of colors compared to those seen under the standard daylight D65 without the glazing. In general, it is calculated as an average value from eight selected colors [32]:

$$R_a = \frac{1}{8}\sum_{i=1}^{8}\left\{100 - 4.6\left[\sum_{X=U,V,W}\left(X_{t,i}^* - X_{r,i}^*\right)^2\right]^{1/2}\right\} \quad (5)$$

where $\left(U_{t,i}^*, V_{t,i}^*, W_{t,i}^*\right)$ and $\left(U_{r,i}^*, V_{r,i}^*, W_{r,i}^*\right)$ are the color space coordinates for the eight test colors illuminated with and without interposed window, respectively.

Figure 8 shows the luminous and colorimetric characteristics obtained from the transmittance and reflectance spectra represented in Fig. 5 for the glass/SnO_x/Ag/SnO_x samples with various Ag thicknesses, applying the spectral functions illustrated in Fig. 7. The highest luminous transmittance ($\tau_L = 84\%$) is achieved for a 15 nm-thick silver film, which gives minimum luminous reflectance $\rho_L = 8\%$ and excellent color rendering $R_a = 98\%$. High luminous and color performance is also achieved by increasing the silver film thickness to 18 nm ($\tau_L = 81\%$, $R_a = 96\%$), but a further increase to 21 nm thickness produces a significant worsening ($\tau_L = 61\%$, $R_a = 89\%$) that is related to the increment in the Ag extinction coefficient. Otherwise, it should be noted that SnO_x/Ag/SnO_x coatings allow achieving better visible characteristics than analogous SnO_x films without the Ag interlayer (i.e., $t_{Ag} = 0$ in Fig. 8). In general, it can be thought that values of τ_L as high as possible are preferably, comparable to ordinary glazing ($\tau_L = 91\%$, $R_a = 99\%$ for the bare glass substrate). Nevertheless, different optimal values have been suggested depending on the climate region ($\tau_L > 70\%$ for temperate and cool climates, $\tau_L > 60\%$ for hot climate) in order to reduce the building energy consumption associated to heating and/or cooling loads along with the artificial lighting demands [5, 33].

For thermal performance characterization, the heat reflectance (ρ_H) is commonly used [1, 2, 10, 14]. This is calculated as the fraction of the incident radiation that is reflected by the glazing in the infrared range:

$$\rho_H = \frac{\sum_{\lambda=0.78\mu m}^{2.50\mu m} R(\lambda)\Delta\lambda}{\sum_{\lambda=0.78\mu m}^{2.50\mu m} \Delta\lambda} \quad (6)$$

which allows to estimate the emissivity value as [3]:

$$\varepsilon = 1 - \rho_H \quad (7)$$

Emissivity alone cannot describe the overall energy efficiency of a building element. Moreover, energy building designs are based on the solar factor (solar heat gain coefficient or g-value) [3, 5, 34] that represents the total solar energy transmitted indoors through the glazing, both by direct solar transmission (τ_S) and by the indoor emission of part of the absorbed solar energy (α_S) [35]:

$$g = \tau_S + \alpha_S \frac{h_i}{h_i + h_e} \quad (8)$$

where h_i and h_e are the internal and external heat transfer coefficients, respectively, being $h_i = 7.7$ W/(m^{2}K) and $h_e = 25.0$ W/(m^{2}K) the standard values according to the European normative [36]. A previous step is to calculate the solar transmittance, reflectance and absorptance by taking the whole wavelengths range for the normalized solar spectrum S:

$$\tau_S = \frac{\sum_{\lambda=0.30\mu m}^{2.50\mu m} T(\lambda)S(\lambda)\Delta\lambda}{\sum_{\lambda=0.30\mu m}^{2.50\mu m} S(\lambda)\Delta\lambda} \quad (9a)$$

$$\rho_S = \frac{\sum_{\lambda=0.30\mu m}^{2.50\mu m} R(\lambda)S(\lambda)\Delta\lambda}{\sum_{\lambda=0.30\mu m}^{2.50\mu m} S(\lambda)\Delta\lambda} \quad (9b)$$

$$\alpha_S = 1 - \tau_S - \rho_S \quad (9c)$$

Selectivity index, defined as the ratio of luminous transmittance with total energy transmittance (τ_L/g), is often used in glass industry. It can be considered as a figure of merit for glazing comparison, because high selective coefficients are better for solar control performance [35].

The emissivity and solar heat gain values corresponding to the glass/SnO$_x$/Ag/SnO$_x$ samples with various Ag interlayer thicknesses are represented in Fig. 9. Both emissivity and solar gain decrease as the silver thickness increases, with $\varepsilon < 0.48$ and $g < 0.65$ for $t_{Ag} > 12$ nm. The lowest values, $\varepsilon = 0.04$ and $g = 0.23$, are obtained for the thickest metal interlayer $t_{Ag} = 24$ nm. As mentioned above, optimal windows must have different properties for various climates. About the solar gain required for efficient energy performance, it is estimated to be more restrictive for hot regions ($g < 0.4$) than for temperate and cold climates ($g = 0.5$–0.6) [5, 33].

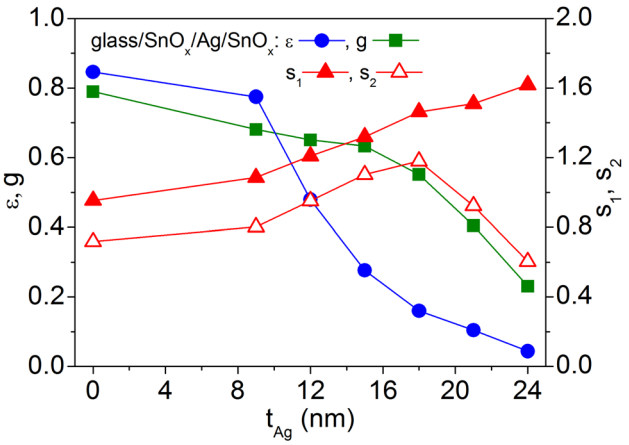

Fig. 9 Emissivity, solar heat gain and selectivity indexes calculated for three-layer coatings on glass substrates, with 30 nm-thick SnO$_x$ films on both sides and different thickness for the Ag interlayer

Concerning the selectivity index, it was first calculated as the simplest ratio [35]:

$$s_1 = \frac{\tau_L}{g} \quad (10a)$$

The results plotted in Fig. 9 show that the highest s_1 value occurs at the highest silver film thickness, which reduces the luminous transmittance to only 37% (Fig. 8). Such luminous transmittance is too low for practical glazing applications, which makes us think that the definition given in Eq. (10a) weights s_1 excessively in favor of the solar gain. A better balance between luminous transmittance and solar heat gain can be achieved by redefining the figure of merit as proposed for other applications [37]. For transparent thin-film electrodes, Haacke defined a figure of merit proportional to a power of the optical transmittance [37], $T^n = (e^{-\alpha t})^n$, being α the absorption coefficient of the film with t thickness. Besides, n is a number that can take different values setting the film thickness and transmittance limits that maximize the function: $t_{max} = 1/(n\alpha)$, for which $T = e^{-1/n}$. Thus, values of n equal to 2, 4, 8 or 10 place the maximum at transmittances of 61%, 78%, 88% or 90%, respectively. For building glazing, the luminous transmittance limit can be set at 60% [33] and therefore a value of $n = 2$ has been selected to compare the present samples with an alternative selective index:

$$s_2 = \frac{\tau_L^2}{g} \quad (10b)$$

Effectively, the application of Eq. (10b) in Fig. 9 gives a maximum s_2 value for the three-layer coating with 18 nm-thick silver, corresponding to luminous transmittance and solar heat gain values ($\tau_L = 81\%$, $g = 0.55$) considered optimal

for efficient glazing in temperate and cold climates. Besides, a slight increment in the Ag interlayer thickness to 21 nm makes these parameters decrease to a level ($\tau_L = 61\%$, $g = 0.40$) that is considered more suitable for heat mirrors in hot regions [5, 33].

4 Conclusions

SnO_x/Ag/SnO_x multilayer coatings prepared by DC sputtering on glass substrates are proven suitable for energy-efficient windows by adjusting properly the deposition conditions.

During the tin oxide growth from a pure Sn target, the oxygen to argon partial pressure ratio must be maintained low enough to avoid silver oxidation. This results in SnO_x films with a relatively high refractive index ($n \sim 2.5$ at $\lambda = 0.55$ µm), which allows reducing the dielectric thickness required for optimum three-layer performance. Symmetrical configurations with 30 nm-thick SnO_x films on both sides have given the best fits of the transmittance spectra to the photopic vision function (with the maximum located at $\lambda = 0.55$ µm).

The silver interlayer should be kept between 15 and 18 nm in thickness for achieving a considerable heat reflectance ($\rho_H = 75$–85%) while maintaining the luminous transmittance above 80% with an excellent color rendering above 96%. For thicker Ag films, both the bandwidth and the intensity of the visible transmittance decrease due to the increment in the extinction coefficient.

The usual selectivity index, defined as the ratio of luminous transmittance to solar heat gain (τ_L/g), provides a maximum for the multilayer coating with 24 nm-thick Ag. This corresponds to minimal emissivity and solar gain ($\varepsilon = 0.04$, $g = 0.23$), but also to a luminous transmittance $\tau_L = 37\%$ that is too low for most glazing applications. Therefore, the figure of merit has been redefined as τ_L^2/g, which gives a maximum for 18 nm-thick Ag, corresponding to values of $\tau_L = 81\%$ and $g = 0.55$ that are considered optimal for energy-efficient windows in temperate and cold climates.

Acknowledgments This work has been carried out in the frame of the EFOX project.

Compliance with ethical standards

Conflict of interest The authors declare that they have no Conflict of interest.

References

1. Dalapati GK, Kushwaha AK, Sharma M, Suresh V, Shannigrahi S, Zhuk S et al (2018) Transparent heat regulating (THR) materials and coatings for energy saving window applications: impact of materials design, micro-structural, and interface quality on the THR performance. Prog Mater Sci 95:42–131. https://doi.org/10.1016/j.pmatsci.2018.02.007
2. Nezhad EH, Haratizadeh H, Kari BM (2019) Influence of Ag mid-layer in the optical and thermal properties of ZnO/Ag/ZnO thin films on the glass used in Buildings as insulating glass unit (IGU). Ceram Int 45:9950–9954. https://doi.org/10.1016/j.ceramint.2019.02.037
3. Jelle BP, Kalnæs SE, Gao T (2015) Low-emissivity materials for building applications: a state-of-the-art review and future research perspectives. Energy Build 96:329–356. https://doi.org/10.1016/j.enbuild.2015.03.024
4. Granqvist CG, Niklasson GA (2018) Solar energy materials for thermal applications: a primer. Sol Energy Mater Sol Cells 180:213–226. https://doi.org/10.1016/j.solmat.2018.02.004
5. Rezaei SD, Shannigrahi S, Ramakrishna S (2017) A review of conventional, advanced, and smart glazing technologies and materials for improving indoor environment. Sol Energy Mater Sol Cells 159:26–51. https://doi.org/10.1016/j.solmat.2016.08.026
6. Guillén C, Herrero J (2016) Comparing the plasmonic characteristics of sputtered ZnO: Al and I_n2_O3: Sn thin films as a function of the heating temperature and atmosphere. Thin Solid Films 605:136–142. https://doi.org/10.1016/j.tsf.2015.09.071
7. Guillén C, Herrero J (2013) Plasmonic characteristics of Ag and ITO/Ag ultrathin films as-grown by sputtering at room temperature and after heating. J Phys D Appl Phys 46:295302. https://doi.org/10.1088/0022-3727/46/29/295302
8. Zhou H, Yu SJ, Zhang YJ, Chen MG, Jiao ZW, Si PZ (2013) In situ electric properties of Ag films deposited on rough substrates. Philos Mag Lett 93:18–26. https://doi.org/10.1080/09500839.2012.728297
9. Wei H, Eilers H (2009) From silver nanoparticles to thin films: Evolution of microstructure and electrical conduction on glass substrates. J Phys Chem Solids 70:459–465. https://doi.org/10.1016/j.jpcs.2008.11.012
10. Al-Kuhaili MF, Ahmad SHA, Durrani SMA, Faiz MM, Ul-Hamid A (2015) Application of nickel oxide thin films in NiO/Ag multilayer energy-efficient coatings. Mater Sci Semicond Process 39:84–89. https://doi.org/10.1016/j.mssp.2015.04.049
11. Kato K, Omoto H, Tomioka T, Takamatsu A (2011) Visible and near infrared light absorbance of Ag thin films deposited on ZnO under layers by magnetron sputtering. Sol Energy Mater Sol Cells 95:2352–2356. https://doi.org/10.1016/j.solmat.2011.04.005
12. Durrani SMA, Khawaja EE, Al-Shukri AM, Al-Kuhaili MF (2004) Dielectric/Ag/dielectric coated energy-efficient glass windows for warm climates. Energy Build 36:891–898. https://doi.org/10.1016/j.enbuild.2004.02.003
13. Guillén C, Herrero J (2011) TCO/metal/TCO structures for energy and flexible electronics. Thin Solid Films 520:1–17. https://doi.org/10.1016/j.tsf.2011.06.091
14. Yoldas BE, O'Keefe T (1984) Deposition of optically transparent IR reflective coatings on glass. Appl Opt 23:3638. https://doi.org/10.1364/AO.23.003638
15. Ding G, Clavero C, Schweigert D, Le M (2015) Thickness and microstructure effects in the optical and electrical properties of silver thin films. AIP Adv. https://doi.org/10.1063/1.4936637
16. Bou A, Torchio P, Barakel D, Thoulon PY, Ricci M (2016) Numerical and experimental investigation of transparent and conductive TiOx/Ag/TiOx electrode. Thin Solid Films 617:86–94. https://doi.org/10.1016/j.tsf.2015.12.041
17. Alvarez R, González JC, Espinós JP, González-Elipe AR, Cueva A, Villuendas F (2013) Growth of silver on ZnO and SnO_2 thin films intended for low emissivity applications. Appl Surf Sci 268:507–515. https://doi.org/10.1016/j.apsusc.2012.12.156

18. Pracchia JA, Simon JM (1981) Transparent heat mirrors: influence of the materials on the optical characteristics. Appl Opt 20:251. https://doi.org/10.1364/AO.20.000251
19. Bender M, Seelig W, Daube C, Frankenberger H, Ocker B, Stollenwerk J (1998) Dependence of film composition and thicknesses on optical and electrical properties of ITO-metal-ITO multilayers. Thin Solid Films 326:67–71. https://doi.org/10.1016/S0040-6090(98)00520-3
20. Martín-Palma RJ, Martínez-Duart JM (2002) Ni–Cr passivation of very thin Ag films for low-emissivity multilayer coatings. J Vac Sci Technol A Vac Surf Film 17:3449–3451. https://doi.org/10.1116/1.582081
21. Guillén C, Herrero J (2019) P-type SnO thin films prepared by reactive sputtering at high deposition rates. J Mater Sci Technol 35:1706–1711. https://doi.org/10.1016/j.jmst.2019.03.034
22. Kuamr K, Saboor S, Kumar V, Kim KH, TP AB (2018) Experimental and theoretical studies of various solar control window glasses for the reduction of cooling and heating loads in buildings across different climatic regions. Energy Build 173:326–336. https://doi.org/10.1016/j.enbuild.2018.05.054
23. El Akkad F, Paulose TAP (2014) Optical transitions and point defects in F:SnO_2 films: effect of annealing. Appl Surf Sci 295:8–17. https://doi.org/10.1016/j.apsusc.2013.12.057
24. Ballif C, Moutinho HR, Hasoon FS, Dhere RG, Al-Jassim MM (2000) Cross-sectional atomic force microscopy imaging of polycrystalline thin films. Ultramicroscopy 85:61–71. https://doi.org/10.1016/S0304-3991(00)00043-7
25. European Committee for Standardization (2011) European Standard EN 410:2011. Glass in building. Determination of luminous and solar characteristics of glazing. European Committee for Standardization, Brussels
26. Liang LY, Liu ZM, Cao HT, Shi YY, Sun XL, Yu Z et al (2010) Improvement of phase stability and accurate determination of optical constants of SnO thin films by using Al_2O_3 capping layer. ACS Appl Mater Interfaces 2:1565–1568. https://doi.org/10.1021/am100236s
27. Luo H, Liang L, Cao H (2012) Structural, chemical, optical, and electrical evolution of SnO_x films deposited by reactive rf magnetron sputtering. ACS Appl Mater Interfaces 4:5673. https://doi.org/10.1021/am301601s
28. Niklasson GA, Granqvist CG, Hunderi O (1981) Effective medium models for the optical properties of inhomogeneous materials. Appl Opt 20:26. https://doi.org/10.1364/ao.20.000026
29. Leftheriotis G, Yianoulis P, Patrikios D (1997) Deposition and optical properties of optimised ZnS/Ag/ZnS thin films for energy saving applications. Thin Solid Films 306:92–99. https://doi.org/10.1016/S0040-6090(97)00250-2
30. Al-Kuhaili MF, Al-Aswad AH, Durrani SMA, Bakhtiari IA (2009) Transparent heat mirrors based on tungsten oxide-silver multilayer structures. Sol Energy 83:1571–1577. https://doi.org/10.1016/j.solener.2009.05.006
31. Gueymard CA, duPont WC (2009) Spectral effects on the transmittance, solar heat gain, and performance rating of glazing systems. Sol Energy 83(2009):940–953. https://doi.org/10.1016/j.solener.2008.12.012
32. International Commission on Illumination, Report CIE 13.3:1995. Method of Measuring and Specifying Colour Rendering Properties of Light Sources, (1995).
33. Piccolo A, Simone F (2015) Performance requirements for electrochromic smart window. J Build Eng 3:94–103. https://doi.org/10.1016/j.jobe.2015.07.002
34. Chow T, Li C, Lin Z (2010) Innovative solar windows for cooling-demand climate. Sol Energy Mater Sol Cells 94:212–220. https://doi.org/10.1016/j.solmat.2009.09.004
35. Ghosh A, Mallick TK (2018) Evaluation of optical properties and protection factors of a PDLC switchable glazing for low energy building integration. Sol Energy Mater Sol Cells 176:391–396. https://doi.org/10.1016/j.solmat.2017.10.026
36. European Committee for Standardization (2011) European Standard EN 673:2011. Glass in building. Determination of thermal transmittance (U value). Calculation method. German Institute for Standardization, Berlin
37. Haacke G (1976) New figure of merit for transparent conductors. J Appl Phys 47:4086–4089. https://doi.org/10.1063/1.323240